JACS
JOURNAL OF THE AMERICAN CHEMICAL SOCIETY
Article
pubs.acs.org/JACS

The Central Role of Bicarbonate in the Electrochemical Reduction of Carbon Dioxide on Gold

Marco Dunwell,[†,∥] Qi Lu,[†,‡,∥,§] Jeffrey M. Heyes,[†] Jonathan Rosen,[†] Jingguang G. Chen,[‡] Yushan Yan,*[,†] Feng Jiao,*[,†] and Bingjun Xu*[,†]

[†]Center for Catalytic Science and Technology, Department of Chemical and Biomolecular Engineering, University of Delaware, Newark, Delaware 19716, United States

[‡]Department of Chemical Engineering, Columbia University, New York, New York 10027, United States

Supporting Information

ABSTRACT: Much effort has been devoted in the development of efficient catalysts for electrochemical reduction of CO_2. Molecular level understanding of electrode-mediated process, particularly the role of bicarbonate in increasing CO_2 reduction rates, is still lacking due to the difficulty of directly probing the electrochemical interface. We developed a protocol to observe normally invisible reaction intermediates with a surface enhanced spectroscopy by applying square-wave potential profiles. Further, we demonstrate that bicarbonate, through equilibrium exchange with dissolved CO_2, rather than the supplied CO_2, is the primary source of carbon in the CO formed at the Au electrode by a combination of in situ spectroscopic, isotopic labeling, and mass spectroscopic investigations. We propose that bicarbonate enhances the rate of CO production on Au by increasing the effective concentration of dissolved CO_2 near the electrode surface through rapid equilibrium between bicarbonate and dissolved CO_2.

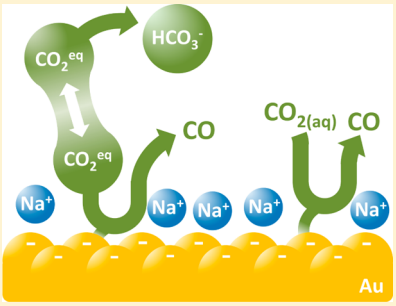

INTRODUCTION

As atmospheric CO_2 levels passed 400 ppm in March 2015,[1] it is clear that curbing anthropogenic CO_2 emissions alone is not sufficient to address the concern over climate change. Efficient CO_2 capture and conversion strategies are needed.[2,3] To this end, renewable electricity coupled with CO_2 electrochemical reduction as a platform of artificial photosynthesis is a promising approach.[4] Technologies for CO_2 utilization as such have the potential to not only reduce CO_2 concentration in the atmosphere, but to supplement, if not eventually replace, diminishing fossil fuel reserves.[5−7] Nevertheless, an efficient and cost-effective synthetic scheme for converting CO_2 into fuels and commodity chemicals remains elusive. Breakthroughs in the development of active, selective, and stable electrocatalysts for CO_2 reduction are acutely needed for both electrochemical and photoelectrochemical approaches. A key barrier in developing such electrocatalysts is the lack of molecular level knowledge of surface-mediated electrochemical reactions. The wide variety of possible products (number of electrons transferred) ranging from CO and HCOOH (2 e^-) up to $CH_3CH_2CH_2OH$ (18 e^-) in the electrochemical CO_2 reduction reaction (CO_2RR) pose significant difficulties in elucidating reaction mechanisms.[8,9] Another compelling challenge lies in obtaining spectroscopic information selectively on the electrode surface because most CO_2RRs are conducted in aqueous solutions and the strong absorption of water could easily overwhelm signals from the electrochemical interface. Therefore, mechanistic investigations of the CO_2RR on electrode materials known to only produce one or few products with surface sensitive techniques is a logical and important step in understanding the surface-mediated CO_2RR.

Au is known as a highly efficient and selective catalyst in the electrochemical CO_2RR for CO production, a reaction heavily investigated in recent years as an alternative, carbon-negative route to produce syngas components.[10−14] This reaction is also of enormous fundamental importance because it is believed to be the first step in the reduction of CO_2 to higher value products such as hydrocarbons and oxygenates.[8,15] Attenuated total reflectance−surface enhanced infrared absorption spectroscopy (ATR-SEIRAS) is a vibrational spectroscopic technique that selectively detects species adsorbed on and near (<10 nm) the metal surface.[16−19] The contribution of the spectroscopic signal decreases exponentially as the distance between the molecule and the metal surface grows; therefore, it is an ideal tool to probe a variety of electrochemical processes. Previous reports have leveraged this technique for the study of various important electrochemical processes such as methanol oxidation,[20] ammonia oxidation,[21] hydrogen oxidation/evolution,[22−24] and the CO_2RR on Cu electrodes.[25,26] Additionally, Wuttig et al. employed ATR-SEIRAS in investigation of the electroreduction of CO_2 on Au film electrodes;[19] however, contamination of the Au working electrode by Pt, likely due to the electrochemical deposition of dissolved Pt from the counter electrode on to the cathodic working electrode, complicates the assignments of observed CO bands and leads to the erroneous conclusion that an irreversibly adsorbed bridge-bonded CO

Received: December 26, 2016
Published: February 17, 2017

DOI: 10.1021/jacs.6b13287
J. Am. Chem. Soc. 2017, 139, 3774−3783

poisons the Au surface. In this work, we report the first mechanistic study of the CO_2RR on a contaminant-free Au surface in an aqueous electrolyte using a combination of in situ ATR-SEIRAS, isotopic labeling, and mass spectrometric techniques. By applying a square-wave potential profile, in which CO is produced at the low potential, then reabsorbed at the high potential where it can be observed using ATR-SEIRAS, we demonstrate that invisible reaction intermediate (adsorbed CO) on Au under typical CO_2RR conditions can be directly observed with in situ vibrational spectroscopy. Further, based on spectroscopic observations and rigorous kinetic studies, we propose for the first time that HCO_3^-, in addition to acting as a pH buffer[8] or proton donor[27] as previously proposed, acts to increase the effective CO_2 concentration in solution through rapid equilibrium between the two species.

EXPERIMENTAL SECTION

Materials. Au film electrodes were deposited directly on the reflecting plane of a Si prism using a modified electroless chemical deposition method outlined by Miyake et al.[28] The prism was first polished with a 0.05 μm Al_2O_3 slurry and sonicated in acetone and water to remove the residue. After polishing, the Si prism was immersed in a 3:1 by volume solution H_2SO_4 (Sigma-Aldrich, 95−98%) and H_2O_2 (Sigma-Aldrich, 30%) for 20 min in order to clean the prism of organic contaminants. Following cleaning, the reflecting plane of the prism was immersed in NH_4F (Sigma-Aldrich, 40%) for 90−120 s to remove the oxide layer and create a hydrogen-terminated surface to improve adhesion of the Au film.[29] The Si surface was then immersed in a 4.4:1 by volume mixture of 2% HF and Au plating solution consisting of 5.75 mM $NaAuCl_4{\cdot}2H_2O$, 0.025 M NH_4Cl, 0.075 M Na_2SO_3, 0.025 M $Na_2S_2O_3{\cdot}5H_2O$, and 0.026 M NaOH for 4 min. To prepare electrodes for isotopically labeled electrolysis experiments, bulk Au foil was purchased from Alfa Aesar (99.999%) and was polished with sandpapers (400 and 800 Grit). The Au foil was then cut into pieces with dimensions of 15 mm × 5 mm. Finally, a nickel wire was connected to one end of the gold piece via spot-welding. The electrode was then etched in aqua regia for 30 s and rinsed using double deionized−distilled water (Barnstead Mega-Pure Water Purification System) for subsequent electrochemical studies. $NaHCO_3$ electrolyte was prepared by purging a solution made from Na_2CO_3 (Fluka, ≥99.9999%) overnight with high purity CO_2 gas (Matheson, 99.999%) until the solution pH had reached 7.2, indicating full conversion of Na_2CO_3 to $NaHCO_3$.[19,27,30] The electrolyte was purified using a solid-supported iminodiacetate resin (Chelex 100, Sigma-Aldrich) in order to prevent any potential impurity metal deposition and achieve a sustainable catalytic surface during CO_2RR.[31]

In Situ ATR-SEIRAS Experiments. A polycrystalline Au nanofilm, deposited chemically on the reflecting plane of a Si prism cut to a 60° angle of incidence, served as the working electrode. A two-compartment spectroelectrochemical cell, separated by an anion-exchange membrane (Fumasep, FAA-3-PK-130), was designed to accommodate the Si prism and to avoid any possible cross-contamination from the counter electrode (Figure S1a). A graphite rod, rather than a Pt foil/wire, was used as the counter electrode to avoid any possible Pt contamination on the working electrode (Figure S1b) as demonstrated previously in studies of the hydrogen evolution reaction using non-Pt based cathodes.[32−34] The electrolytes used in all spectroelectrochemical experiments were prepared by the same method as for electrolysis on bulk Au foils outlined in the previous section. ATR-SEIRAS experiments were conducted on an Agilent Technologies Cary 660 FTIR spectrometer equipped with a liquid nitrogen-cooled MCT detector and a Pike Technologies VeeMAX II ATR accessory. The spectrometer was coupled with a Solartron SI 1260/1287 system for electrochemical measurements. The reference electrode was an Ag/AgCl electrode (3.0 M KCl, BASi). All spectra were collected with a 4 cm^{-1} resolution with a time resolution of 0.5 s between scans, so that spectra collected using 8 and 64 coadded scans have a time resolution of roughly 4 and 32 s, respectively. Spectra shown in Figure 2 were collected during a potential sweep at 10 mV s^{-1}, so that each spectrum was an average over ∼40 mV. All other spectra shown were collected at a constant potential. Spectra are presented in absorbance units where positive and negative peaks signify an increase and decrease in the interfacial species, respectively. All potentials are given on the reversible hydrogen electrode (RHE) scale unless noted otherwise.

Electrochemical Kinetics Experiments. A Princeton Applied Research VersaSTAT 3 potentiostat was used for isotopically labeled electrolysis experiments. Electrolysis was performed under room temperature in a gastight two-compartment electrochemical cell using a piece of anion exchange membrane (Fumasep, FAA-3-PK-130) as the separator. The working electrode compartment contained 9 mL electrolyte and 9 mL headspace. A graphite rod was used as the counter electrode and Ag/AgCl (3.0 M KCl, BASi) as the reference electrode. Before electrolysis using $^{13}CO_2$, the electrolyte was purged with Ar for at least 1 h to remove the dissolved CO_2 (pH = 8.9 and does not change with longer purging time); in a subsequent step, the electrolyte was purged with $^{13}CO_2$ for 5 min at 5 sccm (pH = 7.2 and does not change with further purging) and the headspace was purged with $^{13}CO_2$ for 5 min. During the electrolysis, the electrolyte in both compartments was stirred at rate of 800 r.p.m. using a magnetic stirrer. Quantification of gas phase products was performed using a gas chromatograph (Agilent, 7890B)/mass spectrometer (Stanford Research Systems, QMS). Gas phase products were collected and injected into the gas chromatograph using a gastight syringe.

RESULTS AND DISCUSSION

Potential-Dependent Behavior of Adsorbed CO on Au. In situ ATR-SEIRAS was used in order to probe the chemically deposited Au electrode surface in a CO_2-saturated 0.5 M $NaHCO_3$ electrolyte as a function of electrode potential (Figure 1). The applied potential was stepped down from 1.0 V to −0.6 V (referenced to RHE unless stated otherwise); however, the adsorbed CO (CO_{ad}) reaction intermediate was only observed in the spectra at ∼2100 cm^{-1} between 0.2 V and

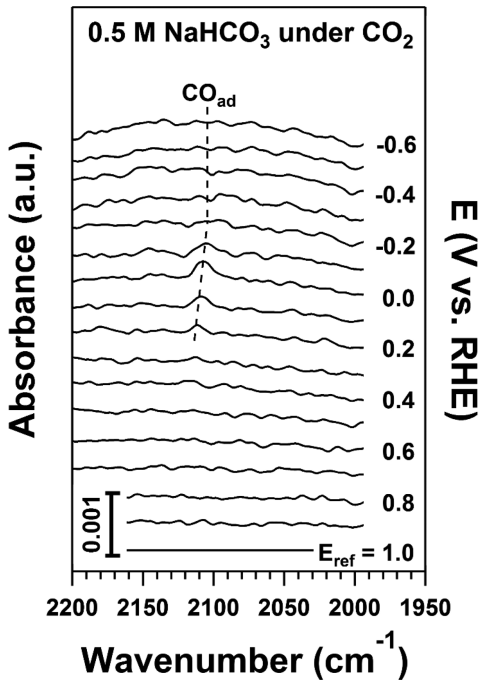

Figure 1. In situ ATR-SEIRAS spectra of adsorbed CO produced in CO_2 saturated 0.5 M $NaHCO_3$ as the potential is stepped in 0.1 V increments from 1.0 to −0.6 V on an Au film electrode. Spectra presented are 64 coadded scans at a 4 cm^{-1} resolution.

DOI: 10.1021/jacs.6b13287
J. Am. Chem. Soc. 2017, 139, 3774−3783

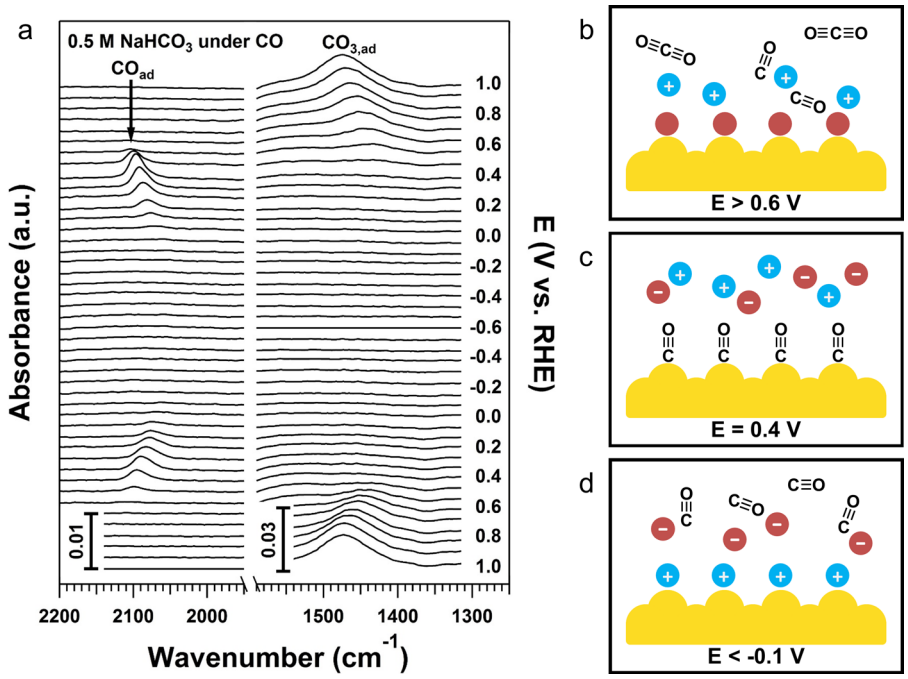

Figure 2. (a) In situ ATR-SEIRAS studies of surface absorbed CO and carbonate. Spectra (8 coadded, 4 cm^{-1} resolution) were collected during potential scans from −0.6 to 1 V at 10 mV/s under 1 atm CO on Au film electrodes in 0.5 M $NaHCO_3$. (b–d) Schematics of proposed CO, (bi)carbonate, and sodium ion behaviors near the electrode surface at different potentials.

−0.1 V,[28,35,36] and was absent between −0.3 V and −0.6 V where the CO_2RR is typically carried out. The standard equilibrium potential for the reduction of CO_2 to CO is −0.11 V,[8] and thus the appearance of the adsorption band as high as 0.2 V is somewhat unexpected. The observation of CO_{ad} at higher than standard equilibrium potential can be explained by a combination of a positive shift in the equilibrium potential due to the low CO partial pressure (no CO was introduced other than that formed in the reaction) according to the Nernst equation. An estimation of the change in equilibrium potential with the coverage of CO_{ad} is provided in the Supporting Information; however, the exact equilibrium potential cannot be obtained without the knowledge of the absolute surface coverage of CO_{ad}. The observation of CO in the spectra despite no significant CO production observed at these potentials using gas chromatography is attributed to the extremely high sensitivity of SEIRAS for CO_{ad}.

To further understand the adsorption behavior of CO on Au and, specifically, and the absence of CO_{ad} at potentials where CO_2 reduction to CO is known to occur, ATR-SEIRAS spectra were collected continuously during potential cycling between 1.0 V and −0.6 V in a CO-saturated 0.5 M $NaHCO_3$ electrolyte (Figure 2a). The single CO_{ad} peak observed from 2050 to 2100 cm^{-1} appears only between −0.1 to 0.6 V, reaching a maximum peak intensity at ∼0.4 V.[28,37,38] The shift in peak position with changing electrode potential can be attributed to the electrochemical Stark effect as demonstrated in SEIRAS studies of CO adsorption.[19,39−42] The CO_{ad} peak decreases concurrently with the rise of a band at ∼1460 cm^{-1} above 0.6 V assigned to adsorbed bicarbonate ($CO_{3,ad}$), which deprotonates upon adsorption.[43] This spectral evidence suggests that the disappearance of CO_{ad} at high potentials may be due to displacement of CO_{ad} by $CO_{3,ad}$ (Figure 2b). It should be noted that oxidation of CO_{ad} to CO_2 also occurs at similar electrode potentials on Au,[44,45] and could also contribute to the disappearance of the CO_{ad} peak above 0.6 V where a positive current is observed (Figure S2). The disappearance of CO_{ad} at lower potentials, where the rate of CO production increases, is less straightforward. We attribute the disappearance of CO_{ad} from the spectra at potentials below −0.1 V to the displacement of CO_{ad} by Na^+ in the outer Helmholtz plane, which are drawn nearer to the electrode surface as the electrode potential decreases.[46] The adsorption of alkali metal cations on metal electrode surfaces at low potentials, and its impact on the rates of electrochemical surface reactions have been discussed in previous reports,[47−49] but experimental investigation of these interactions is less common. One major difficulty in studying alkali cation effects at electrochemical interfaces is that direct observation of these cations is not possible using infrared spectroscopic techniques. In order to overcome this barrier, and to verify that cations in the outer Helmholtz plane are able to displace CO_{ad} at low electrode potentials, the adsorption of CO was studied in a 0.1 M tetramethylammonium iodide (TMAI) saturated with CO using ATR-SEIRAS while the potential was cycled between −0.3 and 0.6 V (Figure S3). The TMA^+ cation was chosen due to the strong spectroscopic signature of the methyl bending mode at 1478 cm^{-1},[50] which increases with decreasing potential, beginning at ∼0.3 V where the CO_{ad} peak intensity begins to decrease. This is strong evidence that cations are able to displace CO_{ad} on Au electrodes at sufficiently low potentials. Similarly, Na^+ cations could reduce the surface coverage of CO_{ad} to below the detection limit of ATR-SEIRAS at low electrode potentials (Figure 2d). It follows that the Au sites will become available once the electrode potential becomes more positive, and CO is free to readsorb on those Au sites provided it is still in the vicinity of the electrode surface (Figure 2c), allowing for observation of CO_{ad} by ATR-SEIRAS.

Contrary to this work and other previous studies of CO adsorption on Au using ATR-SEIRAS in which only a single, linearly bonded CO peak was observed,[28,37,38] some previous

DOI: 10.1021/jacs.6b13287
J. Am. Chem. Soc. 2017, 139, 3774−3783

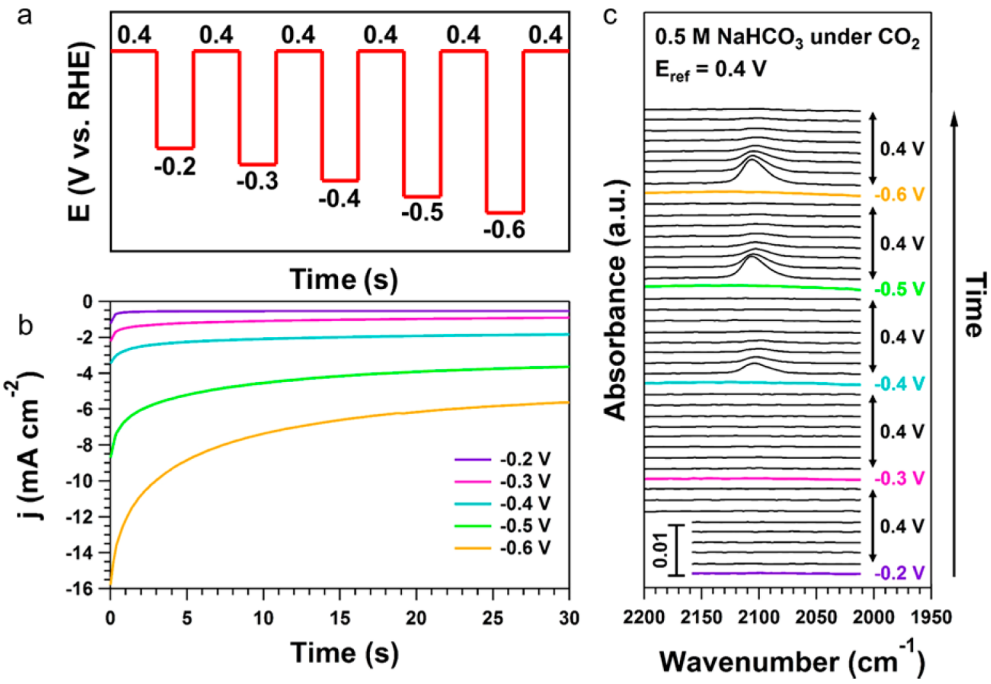

Figure 3. (a) Schematic representation of the potential square-wave electrolysis of CO_2 saturated 0.5 M $NaHCO_3$ on Au film electrodes. (b) Corresponding current profiles at −0.2 V through −0.6 V during electrolysis. (c) ATR-SEIRAS spectra collecting during square-wave electrolysis. Colored spectra were collected during electrolysis at each potential presented in (b). Black traces above each colored spectrum correspond to spectra collected at 0.4 V after each reduction potential. All spectra presented correspond to 8 coadded scans collected with a 4 cm^{-1} resolution.

studies of the CO adsorption on Au using ATR-SEIRAS have observed an additional CO_{ad} peak from ∼1900 cm^{-1} to 2050 cm^{-1} attributed to bridge-bonded CO on Au.[19,39] We believe that the additional CO_{ad} peak is due to contamination of the Au film electrode by Pt dissolution from the counter electrode and electrodeposition on the cathodic working electrode as shown previously for other electrochemical systems with Pt as the counter electrode material.[51−54] This hypothesis was confirmed by studying the adsorption of CO under the same experimental conditions as previously described for the spectra in Figure 2, replacing the graphite rod with a Pt wire counter electrode (Figure S1b). Despite the presence of an anion exchange membrane separating the working and counter electrodes, significant Pt deposition occurs on the Au film working electrode, causing the appearance of additional CO_{ad} bands from 1900 to 2050 cm^{-1} which persist to −0.6 V. Both the peak position and potential range of these additional CO_{ad} bands are in good agreement with CO_{ad} bands observed by Wuttig et al., suggesting that the Au film had significant Pt contamination in their investigation of the CO_2RR on Au.[19] It is important to note that when only a single CO_{ad} band was observed, either an Au counter electrode was used,[28,37] or the potential of the working electrode was maintained above 0.1 V vs RHE,[38] so that the potential of the counter electrode was likely kept sufficiently low, to prevent dissolution of the Pt counter electrode and subsequent electrodeposition on the Au film.

With this insight into the potential-dependent adsorption of CO on Au, a novel spectroelectrochemical method was developed in order to observe, for the first time, the CO_2RR at the potential range in which CO_{ad} is invisible to ATR-SEIRAS under normal conditions. Because the CO intermediate produced at Au electrodes cannot be directly observed during the potentiostatic reduction of CO_2, a potential square-wave electrolysis (illustrated in Figure 3a) alternating between a reduction potential at which the CO_2RR is expected to occur, and 0.4 V, where the CO_{ad} band reaches maximum intensity (Figure 2a) was employed. The potential was held at the reduction potential for 30 s, and stepped to 0.4 V until CO_{ad} desorbs from the electrode. Holding the potential at 0.4 V immediately after electrolysis allows a fraction of CO produced during electrolysis to readsorb to the Au film electrode, enabling direct observation of reduction products. The resultant current profiles during reduction cycles and the corresponding ATR-SEIRAS spectra, collected at an interval of every ∼3 s throughout the square wave experiment, are presented in Figures 3b and 3c. Current densities from −0.2 V and −0.6 V are inflated during the square-wave electrolysis due to the high capacitive current associated with immediately stepping the electrode potential down from 0.4 V, along with the short time scale of the electrolysis. Consistent with the previous results (Figure 1), no CO_{ad} was observed during electrolysis at any potential between −0.2 V and −0.6 V during the square-wave electrolysis. No discernible CO_{ad} peaks were observed in the SEIRAS spectra at 0.4 V after electrolysis at −0.2 V or −0.3 V owing to both the low overpotential for the CO_2RR at these potentials and resulting in the low overall reduction current (<2 mA cm^{-2}, Figure 3b). At reduction potentials of −0.4 V through −0.6 V, however, the rate of CO production is sufficiently high to produce a strong CO_{ad} band at 2106 cm^{-1} after the product readsorbs at 0.4 V. The initial size of the band is a qualitative indicator of the rate of CO production, as the CO_{ad} peak increases in intensity at 0.4 V with decreasing reduction potential due to a higher concentration of produced CO near the Au film following electrolysis. Following the potential step up to 0.4 V, the CO_{ad} peak gradually decreased in intensity as CO concentration near the electrode decreases due to diffusion into to the bulk electrolyte and eventually out of the CO_2-purged solution. This

DOI: 10.1021/jacs.6b13287
J. Am. Chem. Soc. 2017, 139, 3774−3783

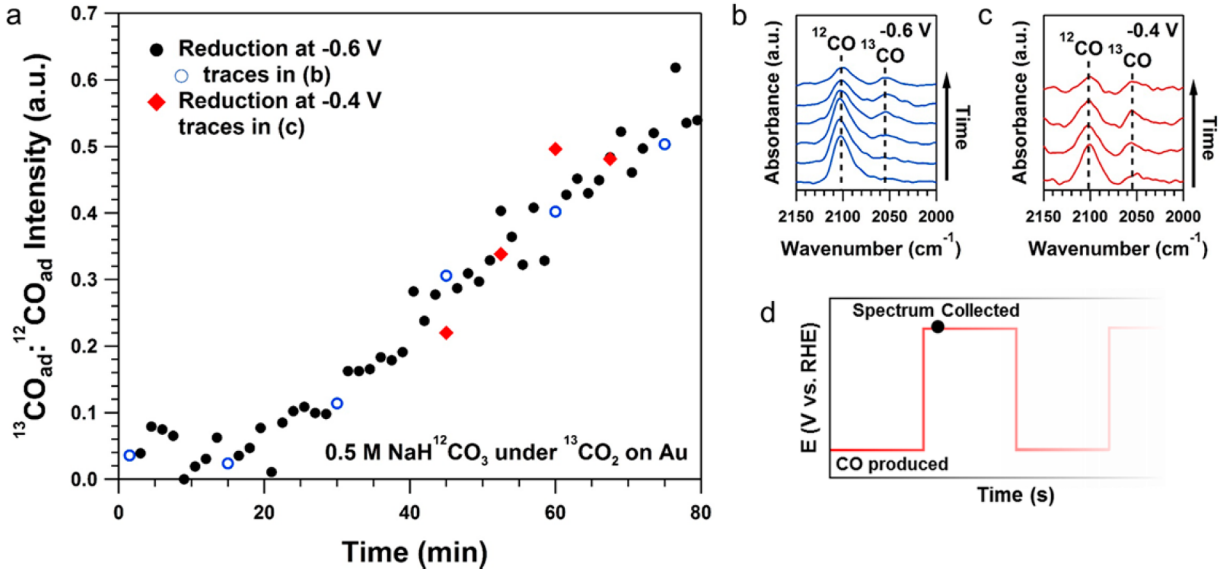

Figure 4. (a) In situ ATR-SEIRAS study of CO produced in the $^{13}CO_2$ purged 0.5 M $NaH^{12}CO_3$ electrolyte in real time. Each point corresponds to the $^{13}CO_{ad}$:$^{12}CO_{ad}$ peak intensity ratio in a single spectrum collected at 0.4 V after reduction at −0.6 V (circles) and −0.4 V (diamonds) on an Au film electrode. (b) Spectra collected at 0.4 V after electrolysis at −0.6 V corresponding to the open blue points in (a). (c) Spectra collected at 0.4 V after electrolysis at −0.4 V corresponding to the red diamonds in (a) and (d) schematic of potential profile used for electrolysis in (a), (b), and (c). All spectra presented correspond to 8 coadded scans collected with a 4 cm^{-1} resolution.

square-wave method enables, for the first time, in situ detection of the CO product of the CO_2RR on Au electrodes.

Isotopic Labeling of Products and Reactants during the CO_2RR. This potential square-wave approach was applied in conjunction with isotopic labeling to gain insights into the CO_2RR mechanism. An isotopically labeled $^{13}CO_2$ purged 0.5 M $NaH^{12}CO_3$ solution was initially reduced at an Au film electrode at −0.6 V, in order to produce CO (Figure 4). The potential was then stepped up to 0.4 V, and a spectrum was collected immediately after the potential step, in order to observe the CO product (Figure 4d). This procedure was repeated continuously over 80 min to investigate the isotopic composition of the CO product as a function of time. The isotopic composition of the produced CO was quantified by monitoring well-defined bands for $^{12}CO_{ad}$ and $^{13}CO_{ad}$ species throughout the electrolysis process. In these experiments a $^{12}CO_{ad}$ peak will appear 2100 cm^{-1},[55] while a peak due to $^{13}CO_{ad}$ is expected to shift to 2053 cm^{-1} based on eq 1, where $1/\lambda$ and $1/\lambda^*$, and μ and μ^* are the wavenumbers of vibrational modes and reduced masses of the unlabeled and labeled molecules, respectively.[56]

$$\frac{1}{\lambda}\sqrt{\frac{\mu^*}{\mu}} = \frac{1}{\lambda^*} \quad (1)$$

Surprisingly, only the unlabeled $^{12}CO_{ad}$ (2100 cm^{-1}) was observed initially (Figures 4a and 4b), demonstrating experimentally, for the first time, that the carbon source of the CO product originates not from the $^{13}CO_2$ in the headspace, but from $H^{12}CO_3^-$ in the electrolyte. A vibrational band corresponding to adsorbed $^{13}CO_{ad}$ (2055 cm^{-1}) appeared after ∼20 min and grew with time as the equilibrium exchange between $^{12}CO_2$ and $H^{13}CO_3^-$ occurred. An experiment conducted at −0.4 V yielded similar results (Figures 4a and 4c). Further, when beginning with $^{12}CO_2$ saturated 0.5 M $NaH^{13}CO_3$ at −0.6 V, the opposite trend of isotopic composition with time was observed (Figure S4), with the majority of the initial product being ^{13}CO. These isotopic labeling studies provide the first experimental evidence that the CO_2 bubbled into the solution is not the primary carbon source for the CO_2RR; rather, carbon in HCO_3^- must be involved and is the primary carbon source.

Two possible mechanisms for the isotopic composition of the CO product could be at play: (i) CO is produced directly from the reduction of $H^{12}CO_3^-$ rather than dissolved $^{13}CO_2$, or (ii) the equilibrium between $CO_{2(aq)}$ and HCO_3^-, i.e.,

$$^{13}CO_{2(aq)} + H^{12}CO_3^- \leftrightarrow {}^{12}CO_{2(aq)} + H^{13}CO_3^-$$

in the electrolyte is sufficiently fast that the isotopic composition of $CO_{2(g)}$ is different than $CO_{2(aq)}$ near the electrode surface where $CO_{2(aq)}$ is reduced. The first possibility was assessed by monitoring the CO production rate during electrolysis at −0.6 V in Ar purged $NaHCO_3$; however, no significant CO product was observed using gas chromatography. This is consistent with previous reports,[27,57] which argue against the first mechanism. We investigated the second possibility further by monitoring the isotopic compositions of the possible carbon sources in the system ($CO_{2(g)}$, $CO_{2(aq)}$, and HCO_3^-) as well as the produced CO using ATR-FTIR and mass spectroscopy (MS). The composition of $^{13}CO_{2(g)}$ and $^{12}CO_{2(g)}$ were estimated by examining gas aliquots from the headspace of the cell using MS, while the composition of bulk $H^{12}CO_3^-$ and $H^{13}CO_3^-$ were estimated through ATR-IR spectrum deconvolution of the vibrational bands associated with $H^{12}CO_3^-$ (1362 cm^{-1})[43] and $H^{13}CO_3^-$ (1323 cm^{-1}). After the $NaH^{12}CO_3$ solution was purged with $^{13}CO_2$ (1 atm), a 5 min electrolysis at −0.6 V was performed. The bicarbonate composition was estimated to be ∼96% $H^{12}CO_3^-$ (*i.e.*, ∼4% $H^{13}CO_3^-$) after purged with $^{13}CO_2$, which decreased to ∼87% after the 5 min electrolysis (Figure 5a and 5b). Correspondingly, the initial composition of CO_2 in the headspace was ∼87% $^{13}CO_2$ (i.e., ∼13% $^{12}CO_2$) and the number gradually decreased to ∼54% during the electrolysis (Figure 5c). The

DOI: 10.1021/jacs.6b13287
J. Am. Chem. Soc. 2017, 139, 3774−3783

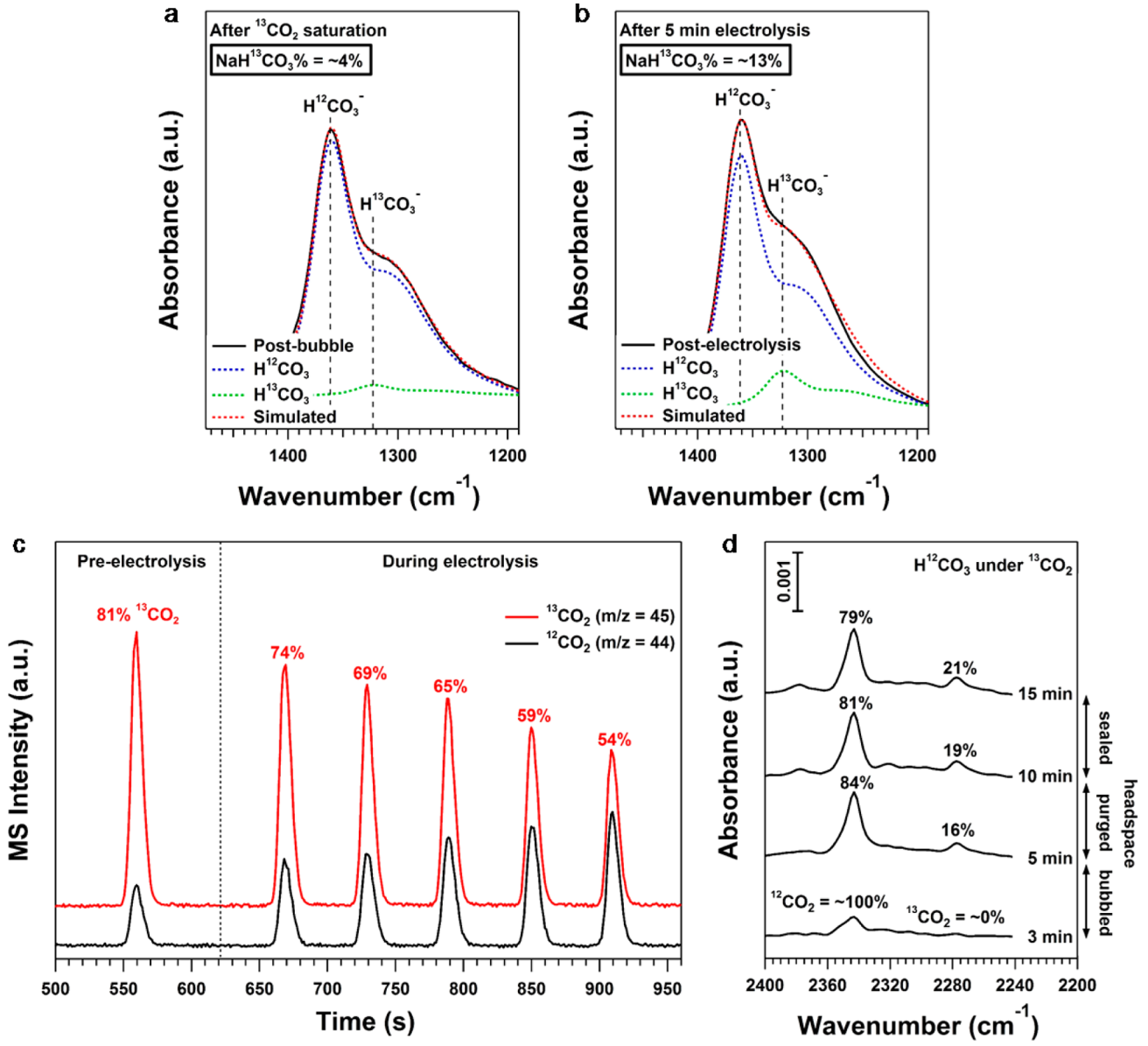

Figure 5. (a) ATR-FTIR spectra (4 cm^{-1} resolution) of $H^{12}CO_3^-$ and $H^{13}CO_3^-$ after electrolyte purging with $^{13}CO_2$ and (b) after 5 min electrolysis. Green and blue traces indicate the portion of the fit (red) composed of $H^{12}CO_3^-$ and $H^{13}CO_3^-$ respectively. Reference spectrum: H_2O. (c) MS spectra indicating the composition of $^{13}CO_{2(g)}$ (red trace, m/z = 29) and $^{12}CO_{2(g)}$ (black trace, m/z = 29) after electrolyte purging and during the 5 min electrolysis. (d) ATR-FTIR spectra (4 cm^{-1} resolution) of $CO_{2(aq)}$ along with percentage of the total peak area belonging to $^{12}CO_{2(aq)}$ and $^{13}CO_{2(aq)}$ in $^{13}CO_2$ purged 0.5 M NaH$^{12}CO_3$. Reference spectrum: Ar saturated 0.5 M NaH$^{12}CO_3$.

isotopic composition of dissolved $CO_{2(aq)}$ was determined using a method similar to bicarbonate in a separate ATR-IR experiment wherein reaction conditions were simulated by beginning with an Ar saturated 0.5 M NaH$^{12}CO_3$ solution and purging the electrolyte with $^{13}CO_2$ for 5 min, then purging the headspace for 5 min, and finally sealing the cell and monitoring the isotopic composition over the next 30 min. Dissolved $^{12}CO_{2(aq)}$ (2343 cm^{-1}) and $^{13}CO_{2(aq)}$ (2278 cm^{-1}) peaks[58] were monitored throughout the experiment and peak areas were calculated in order to determine the isotopic composition of $CO_{2(aq)}$ (Figure 5d). Interestingly, the dissolved $CO_{2(aq)}$ is found to be ~80% $^{12}CO_{2(aq)}$ over the time frame that electrolysis would occur, whereas the $CO_{2(g)}$ in the headspace is only ~36% $^{12}CO_{2(g)}$ over the same time frame (during electrolysis). The $CO_{2(aq)}$ isotopic composition matches much more closely with that of bicarbonate (<10% difference) than $CO_{2(g)}$ (>30% difference), indicating that the equilibrium exchange between bicarbonate and $CO_{2(aq)}$ is very rapid (faster than the diffusion of $CO_{2(g)}$ to become $CO_{2(aq)}$).[59] These results suggest that $CO_{2(g)}$ purged into the system does not remain intact in the electrolyte and is consistent with the CO_2 hydration rate measured by the stopped-flow method.[59] Further, sampling of produced CO in the head space by MS reveals the majority of the carbon monoxide (~89%) produced was ^{12}CO (m/z = 28, Figure 6a), which is similar to the average composition both of $H^{12}CO_3^-$ and $^{12}CO_{2(aq)}$. These MS and FTIR results (summarized in Figure 6b) are consistent with the hypothesis that $CO_{2(g)}$ is not the direct carbon source in the CO_2RR within the duration of this experiment. Instead, carbon atoms in $CO_{2(aq)}$ and HCO_3^- rapidly exchange and equilibrate, and most of carbon in the produced CO originates from HCO_3^- due to its high concentration as compared to $CO_{2(aq)}$.

DOI: 10.1021/jacs.6b13287
J. Am. Chem. Soc. 2017, 139, 3774−3783

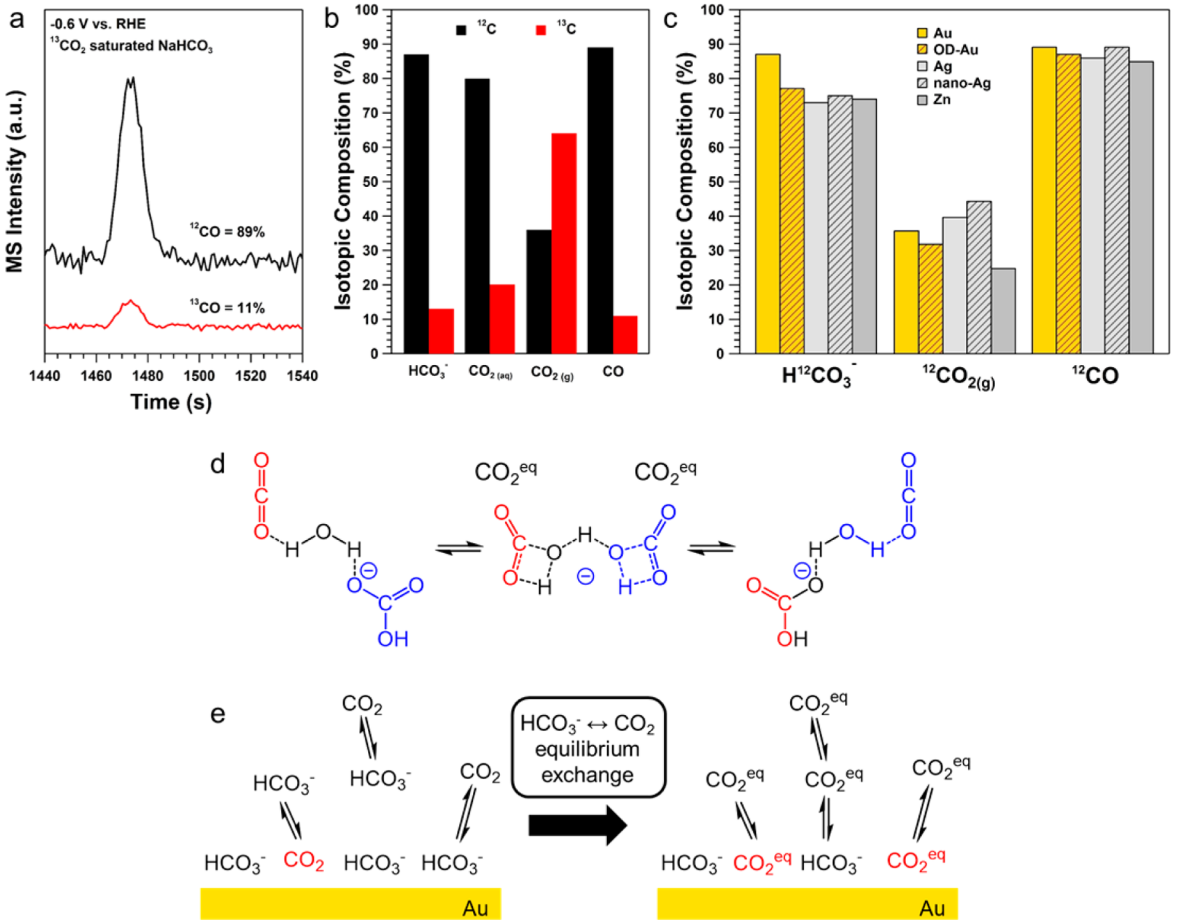

Figure 6. (a) MS spectra of the CO product after 5 min electrolysis in $^{13}CO_2$ saturated $NaH^{12}CO_3$ electrolyte at −0.6 V and corresponding isotopic composition. (b) Summary of the isotopic composition of bicarbonate, CO_2 in the headspace and dissolved in the electrolyte, and CO produced during electrolysis. (c) Summary of the isotopic composition of bicarbonate, $CO_{2(g)}$, and CO on various metal electrodes taken from the full data presented in Figure S5. (d) Proposed equilibrium between CO_2 and bicarbonate. Red, black, and blue colors indicate atoms that were initially part of CO_2, water, and bicarbonate, respectively. (e) Schematic of the proposed mechanism for increasing the effective CO_2 (CO_2^{eq}) concentration via the equilibrium between CO_2 and bicarbonate. Species at the Au surface that can be readily reduced to CO are marked in red.

These isotopically labeled ATR-SEIRAS and MS experiments were repeated (with different electrode potentials, detailed in Figure S5) on other common CO-producing electrodes such as oxide-derived Au,[27] Ag foil,[60−62] nanoporous Ag,[13,30] and Zn foil[60,61,63] to monitor isotopic compositions of $CO_{2(g)}$, bicarbonate, and the CO product (summarized in Figure 6c). All other CO-selective metals tested exhibited similar behavior to that of bulk Au, with the isotopic compositions of bicarbonate consistently falling within 10% of the CO product, with the $CO_{2(g)}$ composition consistently >40% different than CO.

On the basis of the results of isotopic labeling experiments, we propose that the majority of the $CO_{2(aq)}$ being reduced to CO is actually supplied by $H^{12}CO_3^-$ through rapid equilibrium (Figure 6d), and that the primary role of $CO_{2(g)}$ is to establish and maintain the equilibrium concentration of $CO_{2(aq)}$ based on other species in solution. Rapid equilibrium exchange between $CO_{2(aq)}$ and HCO_3^- in solution could increase the effective $CO_{2(aq)}$ concentration (CO_2^{eq}) near the electrode surface by allowing $CO_{2(aq)}$ to hop between bicarbonate ions in solution (analogous to the Grotthuss mechanism[64] for proton diffusion in water in which protons hop between water molecules as Eigen or Zundel cations), essentially allowing any HCO_3^- near the surface to be reduced in the CO_2^{eq} form (Figure 6d). In this case, the role of bicarbonate is not simply a pH buffer[8] or H^+ donor[27] for CO production as previously proposed, but also key to the reaction rate by facilitating $CO_{2(aq)}$ transportation due to its much higher concentration. It is important to clarify that this hypothesis is fundamentally different from claiming that bicarbonate is equivalent to CO_2 in the CO_2RR and can therefore be reduced directly at the electrode surface. If either CO_2^{eq} moiety of the bicarbonate-CO_2 equilibrium complex (Figure 6d) is reduced in the CO_2RR, the other moiety is simultaneously converted to HCO_3^- and can no longer be directly reduced to CO. Considering that this rapid equilibrium is a solution-mediated, rather that electrode mediated process, and the similarity of isotopic labeling results on other CO-selective electrodes, the proposed role of bicarbonate is likely to be general on all CO producing electrodes. This proposed mechanism is in good agreement with previous reports that CO_2RR rates are significantly higher in bicarbonate solutions than other buffer solutions at the similar pH and potential.[8,65] Noda et al.[65] demonstrated that in a 0.1 M phosphate buffer solution of pH = 6.8, the partial CO current density (j_{CO}) is roughly 0.4 mA cm^{-2} at −1.31 V vs RHE. In 0.1 M $KHCO_3$, Hori[61] showed that j_{CO} = 5.0 mA cm^{-2} at the same potential, over an order of magnitude increase in j_{CO} in bicarbonate as compared to that in

DOI: 10.1021/jacs.6b13287
J. Am. Chem. Soc. 2017, 139, 3774−3783

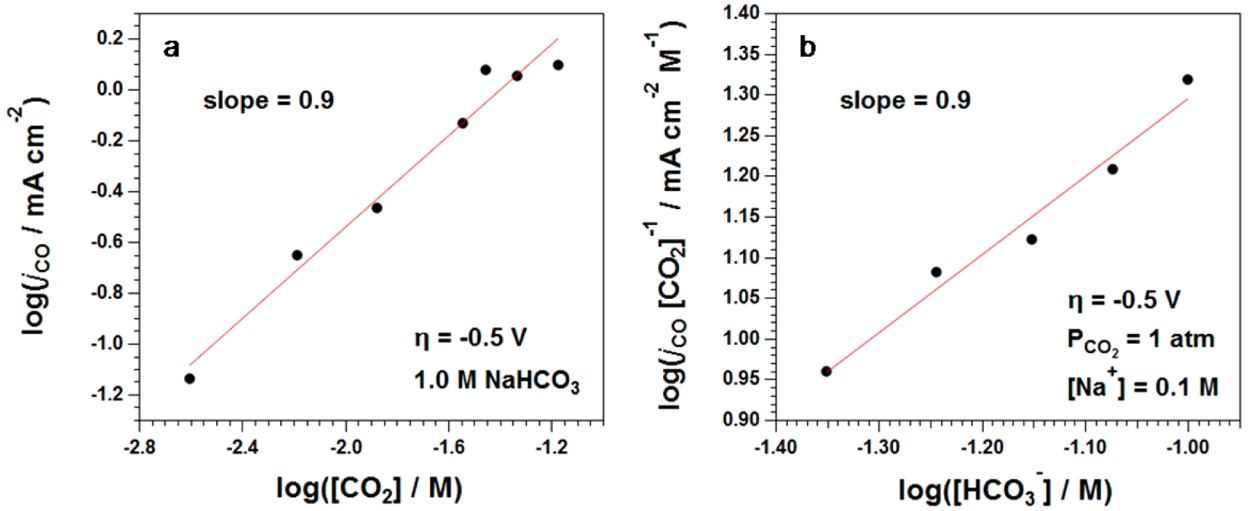

Figure 7. CO partial current density of Au foil vs (a) CO_2 partial pressure in 1.0 M $NaHCO_3$ and (b) $NaHCO_3$ concentration (with Na_2HPO_4 added to the electrolyte to maintain ionic strength and buffer capacity) at 0.1 M Na^+ at a constant overpotential of −0.5 V.

the phosphate buffer solution. The diminished j_{CO} with the phosphate buffer solution argues against the role of bicarbonate as primarily a proton donor in the CO_2RR,[27] because the presence of a more effective proton donor, i.e., H_2PO_4 (pK_a = 7.2), than bicarbonate (pK_a = 10.3) does not translate to higher CO_2RR rates. Furthermore, no spectroscopic evidence for specific adsorption of either bicarbonate or phosphates was observed at CO_2RR potentials (< −0.3 V, Figures 2a and S6), which is likely due to the electrostatic repulsion of between anions and the negatively charged electrode surface.

Kinetic Analysis of the CO_2RR on Au. In light of these new spectroscopic insights, we propose the following modified mechanism for the CO_2RR on Au electrodes in aqueous bicarbonate electrolytes, based on previous work from Rosen et al.[30]

$$CO_{2,eq} + H_2O + * + e^- \leftrightarrow COOH^* + OH^- \quad (2)$$

$$COOH^* + e^- \leftrightarrow CO^* + OH^- \quad (3)$$

$$CO^* \leftrightarrow CO + * \quad (4)$$

In the initial step (eq 2), CO_2, or CO_2^{eq}, is reduced in a simultaneous 1 H^+/ 1 e^- transfer at a free surface site (*) to form the COOH* intermediate. Water is proposed to act as the primary H^+ donor for the reaction, rather than bicarbonate,[27] which will be justified in the following kinetic data. Next, COOH* is reduced in the second electron transfer step to produce adsorbed CO (CO*). CO* then desorbs from the surface to produce the final CO product in eq 4. If we assume low surface coverages of CO* and COOH* ($\theta^* = 1$), as suggested by the lack of SEIRAS signature of adsorbed intermediates at CO_2RR potentials (Figure 1), and eq 3, the second e^- transfer step, to be rate limiting (consistent with the observed Tafel behavior in Figure S7) the CO partial current (i_{CO}) can be described by eq 2:

$$i_{CO} = 2Fk_{2,0}K_1K_\theta a_{CO_2}^{eq} \exp\left(\frac{F(\eta_1^{RHE} - \eta_2^{RHE})}{RT}\right) \quad (5)$$

where $a_{CO_2}^{eq}$ is the activity of CO_2^{eq}, θ_{CO} is surface coverage of CO*, θ_{COOH} is the surface coverage of the COOH* intermediate, $k_{2,0}$ is the rate constant for step (2), K_1 is the equilibrium constant of eq 2, K_θ is $\theta_{CO}/\theta_{COOH}$, η_1^{RHE} and η_2^{RHE} are the applied overpotentials for eqs 2 and 3 on the RHE scale respectively, F is Faraday's constant, R is the gas constant, and T is temperature. The expected Tafel slope ($-\delta E/\delta \log(i_{CO})$) based on eq 5 with the second e^- transfer (eq 3) as the rate-limiting step is 59 mV dec^{-1}, which is in good agreement with the experimentally observed Tafel slope (Figure S7) of 56 mV dec^{-1} at low potentials (−0.325 to −0.4 V) on Au film electrodes.[19] A more detailed derivation of the expected Tafel slope is provided in the "Tafel Slope Derivation" section of the Supporting Information. The Tafel slope increases at potentials below −0.4 V to 250 mV dec^{-1}, which is consistent with previous studies at these higher overpotentials.[19,27] This change in Tafel slope at more negative potentials could be attributed to both a limitation of mass transport of CO_2^{eq} (with currents of −260 μA cm^{-2} at −0.425 V) and/or a blocking of reaction sites by Na^+ in the outer Helmholtz plane.[46] The CO_2RR in aqueous $NaHCO_3$ solutions takes place at potentials lower than −0.11 V vs RHE (the standard equilibrium potential). At these low potentials, the density of cations near the electrode is expected to increase as the electrode becomes more negatively charged. Therefore, we hypothesize that the increase in Tafel slope below −0.4 V is caused by the combined effect of (1) blocking of surface by Na^+ in the outer Helmholtz plane;[46] and (2) electrostatic repulsion of bicarbonate anions from the negatively charged electrode, which limits the ability of CO_2^{eq} to reach the electrode surface.

Dependence of i_{CO} on [CO_2]. To further probe the role of HCO_3^-, reaction orders of both CO_2 and HCO_3^- concentration were studied at a constant overpotential of −0.5 V (i.e., −0.61 V vs RHE). Constant overpotential measurements on the RHE scale are necessary to account for any change in pH that occurs when changing other reaction conditions such as the partial pressure of $CO_{2(g)}$ (p_{CO2}) or concentration of phosphate/carbonate species as detailed by Rosen et al.[30] Unlike previous studies which have investigated CO_2 dependence based on p_{CO2} in the headspace of the electrolysis cell,[27,30,57] CO_2 dependence is investigated using the concentration of $CO_{2(aq)}$ in the solution ([CO_2]) calculated from measured solution pH and equilibria among all dissolved species. As reactions occur in solution, rather than in the gas phase, using [CO_2] rather than p_{CO2} gives a more rigorous

DOI: 10.1021/jacs.6b13287
J. Am. Chem. Soc. 2017, 139, 3774−3783

representation of CO_2 activity for the CO_2RR. Further, the linear correlation between p_{CO2} and $[CO_2]$ based on Henry's law does not hold rigorously due to the equilibrium between $CO_{2(aq)}$ and bicarbonate in the solution. In order to interpret the results of these experiments, eq 5 is expanded to convolute the dependence on $[CO_2]$ and $[HCO_3^-]$ as given in eqs 6 and 7.

$$i_{CO} = 2Fk_{2,0}K_1K_\theta a_{CO_2}\alpha \exp\left(\frac{F(\eta_1^{RHE} - \eta_2^{RHE})}{RT}\right) \quad (6)$$

$$\alpha \propto [HCO_3^-]^\beta \quad (7)$$

where α is a function of $[HCO_3^-]$ and describes the enhancement of $CO_{2(aq)}$ through equilibrium with bicarbonate, and is the order dependence of $[HCO_3^-]$ within α. On the basis of eq 6, the experimentally observed slope of 0.9 from the plot of $\log(j_{CO})$ versus $\log[CO_2]$ (Figure 7a) indicates a first order dependence of i_{CO} on $[CO_2]$, which is consistent with previous reports on Au electrodes.[27,57] A more detailed derivation of the order dependence of $[CO_2]$ and $[HCO_3^-]$ is given in the "Reaction Order Derivation" section of the Supporting Information.

Dependence of i_{CO} on $[HCO_3^-]$. Analysis of the dependence of the reaction rate on $[HCO_3^-]$ is significantly more complex, because $[HCO_3^-]$ is determined via multiple aqueous equilibria, rather than only by the amount of $NaHCO_3$ added. In order to address these complications, the dependence of the reaction rate on $[HCO_3^-]$ is studied by changing $[HCO_3^-]$ while maintaining the ionic strength and buffering capacity of the electrolyte using a phosphate buffer. More specifically, $[Na^+]$ is maintained at 0.1 M, and the ratio between $[HCO_3^-]$ and $[HPO_4^{2-}]$ is varied in order to probe the effect of changing $[HCO_3^-]$. The achievable range of $[HCO_3^-]$ under 1 atm CO_2 is 0.04–0.1 M based on equilibria among $CO_{2(aq)}$, HCO_3^-, HPO_4^{2-}, and $H_2PO_4^-$ (Table S1). If HCO_3^- is indeed only acting as a proton donor[27] or pH buffer[8] in the CO_2RR, replacing the bicarbonate buffer with a phosphate buffer of a similar pH should, in principle, have no effect on the rate of reaction. The results of these experiments are plotted as $j_{CO}[CO_2]^{-1}$ versus $\log[HCO_3^-]$. Since $[CO_2]$ changes with pH, and in turn with the bicarbonate/phosphate ratio, the effect of $[CO_2]$ variation on j_{CO} must be removed from the bicarbonate dependence study by normalizing the j_{CO} with $[CO_2]$ (eq 6). Rather than showing no dependence on $[HCO_3^-]$ ($\beta = 0$), as would be expected if bicarbonate were simply a proton donor, a β value of 0.9 is observed, indicating a first order dependence of i_{CO} on $[HCO_3^-]$ when $[HCO_3^-]$ is between 0.044 and 0.1 M. This observed first order dependence on $[HCO_3^-]$ demonstrates that bicarbonate's primary role in the CO_2RR is not acting as a proton donor or pH buffer, which is consistent with our hypothesis that bicarbonate enhanced CO_2RR rates by increasing the effective $[CO_2]$ near the electrode surface as detailed in eqs 6 and 7. This also justifies the assumption that water, rather than bicarbonate, is the primary proton donor in the proposed mechanism (eqs 2–4).

CONCLUSIONS

In summary, we developed a spectroscopic method to observe normally invisible reaction intermediates of the CO_2RR on Au by ATR-SEIRAS with square-wave potential profiles in which CO is first produced at low electrode potentials (≤ -0.4 V), then observed at 0.4 V. Further, we demonstrate, using a combination of in situ spectroscopic, isotopic labeling, and mass spectrometric techniques, that the majority of $CO_{2(aq)}$ in the electrolyte originates from the equilibrium with bicarbonate rather than diffusion of $CO_{2(g)}$. Rigorous electrokinetic studies also demonstrate a first order dependence on bicarbonate, which supports the conclusion that bicarbonate has a beneficial role in the CO_2RR rather than acting simply as a pH buffer or proton donor. On the basis of these results, we propose that bicarbonate enhances CO_2RR rates by increasing the effective reducible CO_2 concentration in solution through rapid equilibrium exchange between the two species. Isotopic compositions of reactants and products on various electrode materials suggest that this enhancement of CO_2RR rates via rapid equilibrium with bicarbonate is universal to all CO-selective electrodes.

ASSOCIATED CONTENT

Supporting Information

The Supporting Information is available free of charge on the ACS Publications website at DOI: 10.1021/jacs.6b13287.

Additional content including SEIRAS cell setup, cyclic voltammograms, and full ATR-SEIRAS, ATR-FTIR, and MS spectra (PDF)

AUTHOR INFORMATION

Corresponding Authors

*yanys@udel.edu
*jiao@udel.edu
*bxu@udel.edu

ORCID

Feng Jiao: 0000-0002-3335-3203
Bingjun Xu: 0000-0002-2303-257X

Present Address

§Department of Chemical Engineering, Tsinghua University, Haidian, Beijing, China

Author Contributions

‖M.D. and Q. L. contributed equally.

Notes

The authors declare no competing financial interest.

ACKNOWLEDGMENTS

M.D., Y.Y. and B.X. acknowledge the support of National Science Foundation Chemical Catalysis Program (Award No. CHE-1566138). Q.L. acknowledges the support from Fondazione Oronzio e Niccolò De Nora Fellowship. J.R. and F.J. acknowledge the National Science Foundation CAREER Program (Award No. CBET-1350911) for financial support. The Columbia University authors are supported by the US Department of Energy (DE-FG02-13ER16381).

REFERENCES

(1) Earth Systems Research Laboratory, Trends in Atomspheric Carbon Dioxide. http://www.esrl.noaa.gov/gmd/ccgg/trends/index.html, accessed October 2016.

(2) Lewis, N. S.; Nocera, D. G. *Proc. Natl. Acad. Sci. U. S. A.* **2006**, *103* (43), 15729–15735.

(3) Olah, G. A.; Prakash, G. K. S.; Goeppert, A. *J. Am. Chem. Soc.* **2011**, *133* (33), 12881–12898.

(4) Pinaud, B. A.; Benck, J. D.; Seitz, L. C.; Forman, A. J.; Chen, Z.; Deutsch, T. G.; James, B. D.; Baum, K. N.; Baum, G. N.; Ardo, S.; Wang, H.; Miller, E.; Jaramillo, T. F. *Energy Environ. Sci.* **2013**, *6* (7), 1983–2002.

DOI: 10.1021/jacs.6b13287
J. Am. Chem. Soc. 2017, 139, 3774–3783

(5) Aresta, M.; Dibenedetto, A.; Angelini, A. *Chem. Rev.* **2014**, *114* (3), 1709−1742.
(6) Appel, A. M.; Bercaw, J. E.; Bocarsly, A. B.; Dobbek, H.; DuBois, D. L.; Dupuis, M.; Ferry, J. G.; Fujita, E.; Hille, R.; Kenis, P. J. A.; Kerfeld, C. A.; Morris, R. H.; Peden, C. H. F.; Portis, A. R.; Ragsdale, S. W.; Rauchfuss, T. B.; Reek, J. N. H.; Seefeldt, L. C.; Thauer, R. K.; Waldrop, G. L. *Chem. Rev.* **2013**, *113* (8), 6621−6658.
(7) Quadrelli, E. A.; Centi, G.; Duplan, J.-L.; Perathoner, S. *ChemSusChem* **2011**, *4* (9), 1194−1215.
(8) Hori, Y., Electrochemical CO_2 Reduction on Metal Electrodes. In *Modern Aspects of Electrochemistry*; Vayenas, C., White, R., Gamboa-Aldeco, M., Eds.; Springer: New York, 2008; Vol. *42*, pp 89−189.
(9) Kuhl, K. P.; Cave, E. R.; Abram, D. N.; Jaramillo, T. F. *Energy Environ. Sci.* **2012**, *5* (5), 7050−7059.
(10) Asadi, M.; Kumar, B.; Behranginia, A.; Rosen, B. A.; Baskin, A.; Repnin, N.; Pisasale, D.; Phillips, P.; Zhu, W.; Haasch, R.; Klie, R. F.; Král, P.; Abiade, J.; Salehi-Khojin, A. *Nat. Commun.* **2014**, DOI: 10.1038/ncomms5470.
(11) DiMeglio, J. L.; Rosenthal, J. *J. Am. Chem. Soc.* **2013**, *135* (24), 8798−8801.
(12) Kumar, B.; Asadi, M.; Pisasale, D.; Sinha-Ray, S.; Rosen, B. A.; Haasch, R.; Abiade, J.; Yarin, A. L.; Salehi-Khojin, A. *Nat. Commun.* **2013**, DOI: 10.1038/ncomms3819.
(13) Lu, Q.; Rosen, J.; Zhou, Y.; Hutchings, G. S.; Kimmel, Y. C.; Chen, J. G.; Jiao, F. *Nat. Commun.* **2014**, DOI: 10.1038/ncomms4242.
(14) Rosen, B. A.; Salehi-Khojin, A.; Thorson, M. R.; Zhu, W.; Whipple, D. T.; Kenis, P. J. A.; Masel, R. I. *Science* **2011**, *334* (6056), 643−644.
(15) Peterson, A. A.; Abild-Pedersen, F.; Studt, F.; Rossmeisl, J.; Norskov, J. K. *Energy Environ. Sci.* **2010**, *3* (9), 1311−1315.
(16) Osawa, M. *Bull. Chem. Soc. Jpn.* **1997**, *70* (12), 2861−2880.
(17) Osawa, M. Surface-Enhanced Infrared Absorption. In *Near-Field Optics and Surface Plasmon Polaritons*; Kawata, S., Ed.; Springer: Berlin, 2001; Vol. *81*, pp 163−187.
(18) Osawa, M.; Ataka, K.-i.; Yoshii, K.; Yotsuyanagi, T. *J. Electron Spectrosc. Relat. Phenom.* **1993**, *64*−*65* (0), 371−379.
(19) Wuttig, A.; Yaguchi, M.; Motobayashi, K.; Osawa, M.; Surendranath, Y. *Proc. Natl. Acad. Sci. U. S. A.* **2016**, *113* (32), E4585−E4593.
(20) Shao, M. H.; Adzic, R. R. *Electrochim. Acta* **2005**, *50* (12), 2415−2422.
(21) Matsui, T.; Suzuki, S.; Katayama, Y.; Yamauchi, K.; Okanishi, T.; Muroyama, H.; Eguchi, K. *Langmuir* **2015**, *31* (42), 11717−11723.
(22) Kunimatsu, K.; Senzaki, T.; Samjeské, G.; Tsushima, M.; Osawa, M. *Electrochim. Acta* **2007**, *52* (18), 5715−5724.
(23) Kunimatsu, K.; Senzaki, T.; Tsushima, M.; Osawa, M. *Chem. Phys. Lett.* **2005**, *401* (4−6), 451−454.
(24) Kunimatsu, K.; Uchida, H.; Osawa, M.; Watanabe, M. *J. Electroanal. Chem.* **2006**, *587* (2), 299−307.
(25) Heyes, J.; Dunwell, M.; Xu, B. *J. Phys. Chem. C* **2016**, *120* (31), 17334−17341.
(26) Wuttig, A.; Liu, C.; Peng, Q.; Yaguchi, M.; Hendon, C. H.; Motobayashi, K.; Ye, S.; Osawa, M.; Surendranath, Y. *ACS Cent. Sci.* **2016**, *2* (8), 522−528.
(27) Chen, Y.; Li, C. W.; Kanan, M. W. *J. Am. Chem. Soc.* **2012**, *134* (49), 19969−19972.
(28) Miyake, H.; Ye, S.; Osawa, M. *Electrochem. Commun.* **2002**, *4* (12), 973−977.
(29) Nagahara, L. A.; Ohmori, T.; Hashimoto, K.; Fujishima, A. *J. Vac. Sci. Technol., A* **1993**, *11* (4), 763−767.
(30) Wuttig, A.; Surendranath, Y. *ACS Catal.* **2015**, *5* (7), 4479−4484.
(31) Caban-Acevedo, M.; Stone, M. L.; Schmidt, J. R.; Thomas, J. G.; Ding, Q.; Chang, H.-C.; Tsai, M.-L.; He, J.-H.; Jin, S. *Nat. Mater.* **2015**, *14* (12), 1245−1251.
(32) Danilovic, N.; Subbaraman, R.; Strmcnik, D.; Chang, K.-C.; Paulikas, A. P.; Stamenkovic, V. R.; Markovic, N. M. *Angew. Chem., Int. Ed.* **2012**, *51* (50), 12495−12498.
(33) Staszak-Jirkovsky, J.; Malliakas, C. D.; Lopes, P. P.; Danilovic, N.; Kota, S. S.; Chang, K.-C.; Genorio, B.; Strmcnik, D.; Stamenkovic, V. R.; Kanatzidis, M. G.; Markovic, N. M. *Nat. Mater.* **2016**, *15* (2), 197−203.
(34) Chang, S. C.; Hamelin, A.; Weaver, M. J. *J. Phys. Chem.* **1991**, *95* (14), 5560−5567.
(35) Kunimatsu, K.; Aramata, A.; Nakajima, N.; Kita, H. *J. Electroanal. Chem. Interfacial Electrochem.* **1986**, *207* (1), 293−307.
(36) Pronkin, S.; Hara, M.; Wandlowski, T. *Russ. J. Electrochem.* **2006**, *42* (11), 1177−1192.
(37) Pronkin, S.; Wandlowski, T. *Surf. Sci.* **2004**, *573* (1), 109−127.
(38) Sun, S.-G.; Cai, W.-B.; Wan, L.-J.; Osawa, M. *J. Phys. Chem. B* **1999**, *103* (13), 2460−2466.
(39) Lambert, D. K. *Solid State Commun.* **1984**, *51* (5), 297−300.
(40) Lambert, D. K. *Electrochim. Acta* **1996**, *41* (5), 623−630.
(41) Pons, S.; Korzeniewski, C.; Shirts, R. B.; Bewicks, A. *J. Phys. Chem.* **1985**, *89* (11), 2297−2298.
(42) Arihara, K.; Kitamura, F.; Ohsaka, T.; Tokuda, K. *J. Electroanal. Chem.* **2001**, *510* (1−2), 128−135.
(43) Beltramo, G. L.; Shubina, T. E.; Koper, M. T. M. *ChemPhysChem* **2005**, *6* (12), 2597−2606.
(44) Blizanac, B. B.; Arenz, M.; Ross, P. N.; Markovic, N. M. *J. Am. Chem. Soc.* **2004**, *126* (32), 10130−10141.
(45) Dunwell, M.; Wang, J.; Yan, Y.; Xu, B. *Phys. Chem. Chem. Phys.* **2017**, *19* (2), 971−975.
(46) Strmcnik, D.; van der Vliet, D. F.; Chang, K. C.; Komanicky, V.; Kodama, K.; You, H.; Stamenkovic, V. R.; Markovic, N. M. *J. Phys. Chem. Lett.* **2011**, *2* (21), 2733−2736.
(47) Strmcnik, D.; Kodama, K.; van der Vliet, D.; Greeley, J.; Stamenkovic, V. R.; Markovic, N. M. *Nat. Chem.* **2009**, *1* (6), 466−472.
(48) Thorson, M. R.; Siil, K. I.; Kenis, P. J. A. *J. Electrochem. Soc.* **2013**, *160* (1), F69−F74.
(49) Berg, R. W. *Spectrochim. Acta Mol. Biomol. Spectrosc.* **1978**, *34* (6), 655−659.
(50) Cherevko, S.; Keeley, G. P.; Geiger, S.; Zeradjanin, A. R.; Hodnik, N.; Kulyk, N.; Mayrhofer, K. J. J. *ChemElectroChem* **2015**, *2* (10), 1471−1478.
(51) Tian, M.; Cousins, C.; Beauchemin, D.; Furuya, Y.; Ohma, A.; Jerkiewicz, G. *ACS Catal.* **2016**, *6* (8), 5108−5116.
(52) Cherevko, S.; Zeradjanin, A. R.; Keeley, G. P.; Mayrhofer, K. J. J. *J. Electrochem. Soc.* **2014**, *161* (12), H822−H830.
(53) Solla-Gullón, J.; Aldaz, A.; Clavilier, J. *Electrochim. Acta* **2013**, *87*, 669−675.
(54) Miki, A.; Ye, S.; Osawa, M. *Chem. Commun.* **2002**, No. 14, 1500−1501.
(55) Westheimer, F. H. *Chem. Rev.* **1961**, *61* (3), 265−273.
(56) Hori, Y.; Murata, A.; Kikuchi, K.; Suzuki, S. *J. Chem. Soc., Chem. Commun.* **1987**, No. 10, 728−729.
(57) Esler, M. B.; Griffith, D. W. T.; Wilson, S. R.; Steele, L. P. *Anal. Chem.* **2000**, *72* (1), 216−221.
(58) Pocker, Y.; Bjorkquist, D. W. *J. Am. Chem. Soc.* **1977**, *99* (20), 6537−6543.
(59) Hori, Y.; Kikuchi, K.; Suzuki, S. *Chem. Lett.* **1985**, *14* (11), 1695−1698.
(60) Hori, Y.; Wakebe, H.; Tsukamoto, T.; Koga, O. *Electrochim. Acta* **1994**, *39* (11), 1833−1839.
(61) Noda, H.; Ikeda, S.; Oda, Y.; Imai, K.; Maeda, M.; Ito, K. *Bull. Chem. Soc. Jpn.* **1990**, *63* (9), 2459−2462.
(62) Rosen, J.; Hutchings, G. S.; Lu, Q.; Rivera, S.; Zhou, Y.; Vlachos, D. G.; Jiao, F. *ACS Catal.* **2015**, *5* (7), 4293−4299.
(63) Ikeda, S.; Takagi, T.; Ito, K. *Bull. Chem. Soc. Jpn.* **1987**, *60* (7), 2517−2522.
(64) Agmon, N. *Chem. Phys. Lett.* **1995**, *244* (5), 456−462.
(65) Noda, H.; Ikeda, S.; Yamamoto, A.; Einaga, H.; Ito, K. *Bull. Chem. Soc. Jpn.* **1995**, *68* (7), 1889−1895.

DOI: 10.1021/jacs.6b13287
J. Am. Chem. Soc. 2017, 139, 3774−3783